Morphology Control of Electrodeposited Zinc from Alkaline Zincate Solutions for Rechargeable Zinc Air Batteries

Shaigan, N.; Qu, W.; Takeda, T.

Publisher's version / Version de l'éditeur:
https://doi.org/10.1149/1.3507925
ECS Transactions, 28, 32, pp. 35-44, 2010-04-30

ECS Transactions, 28 (32) 35-44 (2010)
10.1149/1.3507925 ©The Electrochemical Society

Morphology Control of Electrodeposited Zinc from Alkaline Zincate Solutions for Rechargeable Zinc Air Batteries

[a]N. Shaigan, [a]W. Qu and [b]T. Takeda

[a]National Research Council Canada, Institute for Fuel Cell Innovation, Vancouver, British Colombia, Canada V6T 1W5

[b]Transport Canada, Ottawa, Ontario, Canada K1A 0N5

Anomalous electrocrystallization of Zn in alkaline electrolytes is one of the hurdles hindering the development and commercialization of secondary alkaline Zn batteries. The issue stems from the fast electrochemical kinetics of Zn in alkaline electrolytes. Pulse deposition enables the use of high peak current densities and overpotentials, increases the nucleation rate and improves the deposit morphology. The cathodic behavior of Zn and effect of pulse parameters including duty cycle and frequency on the deposit morphology were studied for electrolytes containing 4, 6 and 9 M KOH. It was shown that in order to attain fine-grain, smooth deposits by pulse deposition, application of small duty cycles and high frequencies are essential. Pulse deposition, however, does not improve the morphology in case highly concentrated KOH electrolytes are used.

Introduction

In comparison with other anodes used in rechargeable batteries with alkaline electrolytes (i.e., Cd or metal hydride), Zn anodes offer several advantages including low equilibrium potential, high specific volumetric and gravimetric energy, low cost, abundance and being environmentally friendly (1,2). These important characteristics make rechargeable Zn batteries attractive for general applications and particularly for electric vehicles (EVs) where high specific energy and cost are equally critical. Although primary Zn batteries including Zn-air, Zn-Ni, Zn-MnO_2 and Zn-Ag and have been successfully in use for decades, their rechargeable counterparts are not yet able to compete with other commercial secondary batteries due to their poor cycle life.

Upon recharging of a Zn anode, the Zn anodic discharge products, i.e., zincate ions or ZnO, are electrochemically reduced to metallic Zn crystals. In other words, recharging of Zn anodes is an electrodeposition process. In alkaline electrolytes, Zn has a fast electrochemical kinetics that is responsible for its anomalous electrocrystallization. Depending on current density and electrolyte composition, Zn crystals grow with different morphologies categorized as mossy, boulder-like and dendritic all of which become problematic over charge/discharge cycles. In particular, dendrites may puncture the separator and short-circuit the battery. Furthermore, Zn is highly soluble in alkaline electrolyte as zincate complex (i.e., $Zn(OH)_4^{2-}$) that is able to migrate throughout the entire anode mass and electrolyte body. As a result, over the charging, zincates will not

be necessarily reduced on locations where they were originally dissolved from during the discharge. Such behavior results in redistribution of Zn in the anode mass, anode shape changes and isolation of Zn particles from the conductive network. This phenomenon, in turn, leads to densification of the anode, loss of porosity and capacity and accumulation of Zn on the exterior of the anodic mass rather than a uniform distribution. These issues contribute to the poor cycle life of Zn anodes.

The issue of high solubility of Zn in alkaline electrolytes, leading to anode shape changes and redistribution of Zn in the anode mass, has been addressed to some extents by addition of special compounds that reduce or inhibit the dissolution of Zn in alkaline electrolytes. Such compounds can be classified into two categories: chemicals that form insoluble complexes with Zn and those that lower the electrolyte pH and inhibit the formation of soluble zincates. Examples for the former include calcium hydroxide or alkaline fluorides that are usually added to the anode composition and those for the latter are buffering agents including phosphates, borates and arsenides that are added to the electrolyte (2-5).

However, anomalous electrocrystallization of Zn that causes loss of capacity may not be addressed by limiting the solubility of Zn. Pulsating or periodic reverse current deposition is used in general metal electrodeposition to obtain modified, fine-grain deposits with no or minimal need for additives. In this work, the cathodic behavior of Zn and the effect of pulse parameters including duty cycle and frequency on electrocrystallization of Zn in additive-free KOH electrolytes containing dissolved ZnO are studied. The results of this study may be useful for understanding the electrocrystallization behavior of Zn and potential benefits of pulse charging for improved cycle life of alkaline Zn batteries.

Experimental methods

The electrolytes used for the experiments were concentrated aqueous KOH solutions containing dissolved ZnO. The concentrations of KOH were 4, 6 and 9 M for the three different electrolytes. All these electrolytes contained 0.1 M dissolved ZnO. The anodes were pure Zn balls contained in a titanium mesh basket, and electrodeposition was conducted in a 200 mL beaker. The substrates used were 1.27 mm diameter disks punched out of a 100 mesh Cu woven gauze with wire diameter of 0.11 mm. Immediately prior to electrodeposition, substrates were cleaned with acetone, immersed in 50% HCl for 1 minute and rinsed thoroughly with deionized water.

Cathodic polarization curves were obtained with a Solartron SI 1260 using a three-electrode electrochemical cell. The counter electrode was a Pt gauze and working and reference electrodes were pure Zn discs. The electrodes were activated in 10% sulfuric acid and rinsed with deionized water right before each test. Potentiodynamic test with 1 mV S^{-1} scan rate was used to obtain the polarization curves.

Electrodeposition was performed in still condition at room temperature (20±2°C). The power supply used to produce square-wave pulses was a Dynatronix® DuPR.1-.3. Table I lists the pulse parameters used for the experiments. Two different duty cycles and frequencies were chosen. The on-time and off-time were selected so that the area under

each individual pulse (i.e., electric charge) was constant for each of the frequencies regardless of the duty cycle. The off-time, then, remained virtually unchanged for each of the frequencies, and the effect of off-time was almost eliminated. The deposition charge was 78 C equivalent of 26.4 mg Zn (assuming 100% current efficiency) and identical for all of the specimens.

The morphology of Zn deposits was examined by means of scanning electron microscopy (SEM). The instrument used was a Hitachi S-3500N.

TABLE I. Pulse parameter used for the experiments

Duty Cycle[1] θ (%)	Frequency f[2] (Hz)	On-time (ms)	Off-time (ms)	Mean current density (mA cm^{-2})	Peak current density (mA cm^{-2})
				5	**40**
12.5	500	0.25	1.75		
	31.25	4	28		
				5	80
6.25 (6)	500	0.125 (0.12)	1.875 (1.88)		
	31.25	2	30		
100 (DC)	0	1	0	5	5

Results and discussion

Cathodic polarizations

Figure 1 illustrates the cathodic polarization curves for Zn in electrolytes containing different concentrations of KOH. The overpotential for activation-controlled deposition is smaller than approximately 20 mV and a sharp cathodic polarization is observed regardless of the concentration of KOH in the electrolyte. Cachet et al. (6) conducted exhaustive electrochemical impedance measurements for Zn electrode in alkaline solutions and suggested that discharge of Zn in quasi-steady-state is controlled by ion diffusion through a porous surface layer that has a defective ZnO structure with excess of Zn ions. This layer is a mixed conductor, forms near the equilibrium potential and is sharply polarized by either cathodic or anodic polarization (6, 7).

A broad peak is also observed at approximately 40 mV for 6 and 9 M KOH electrolytes and at around 90 mV for 4 M KOH electrolyte. This peak indicated that another reaction, i.e., hydrogen generation, in addition to the reduction of zincate ions occurs in this region of the overpotential.

---

[1] $\theta = \frac{t_{on}}{t_{on} + t_{off}} \times 100$ where t_{on} is the pulse on-time and t_{off} the off-time durations.

[2] $f = \frac{1}{t_{on} + t_{off}} \times 1000 Hz$

For each electrolyte, a current density plateau attributed to the diffusion limiting current density is observed. The value of this limiting current density decreases as the concentration of KOH in the electrolyte increases. As the concentration of KOH increases beyond a certain point, the amount of the free water molecules decreases and the existing water would be only sufficient to hydrate the ions in the electrolyte. Mobility of the ions in the electrolyte, which depends on free water molecules, is then disturbed resulting in lower limiting current densities. Dirske and Hampson showed that the exchange current density of Zn shows a maximum at around 8 M KOH and falls for more concentrated electrolytes due to lack of unbound water molecule and reduced mobility of the ions (8-10).

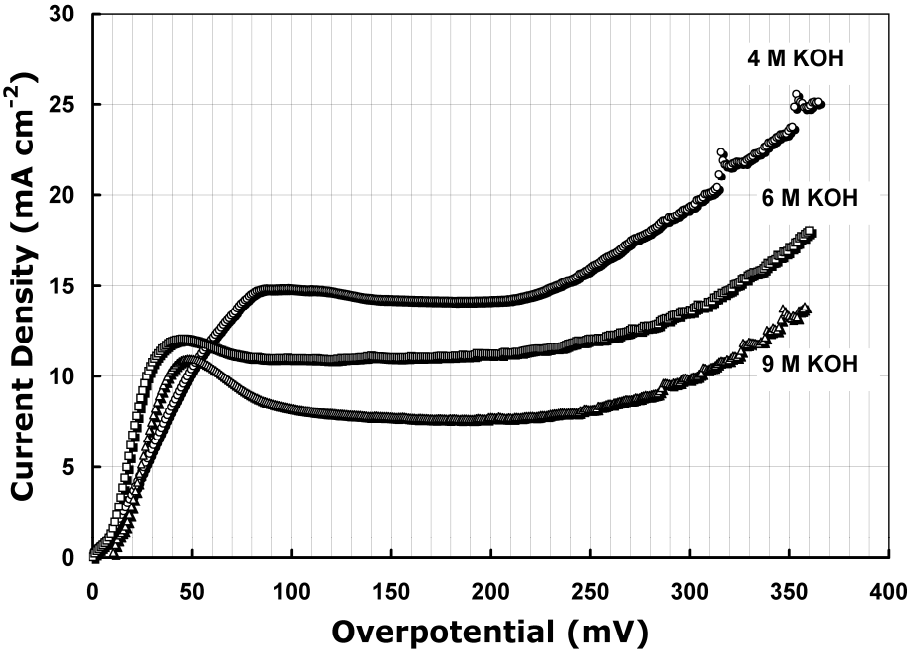

Figure 1. Cathodic polarization curves for Zn electrodes in electrolytes containing 0.1 M ZnO and different concentrations of KOH. The scan rate was 1 mV S^{-1}.

Direct current (DC) deposition

Figure 2 shows the SEM images of Zn deposits obtained in 4, 6 and 9 M KOH electrolytes at the current densities of 5 and 10 mA cm^{-2}. Mossy growth of Zn is clearly observed in Figure 2-a and 2-c that represent deposits obtained from 4 and 6 M KOH electrolyte at 5 mA cm^{-2} current density. A combination of mossy and boulder growth types on convex surface of the wires is seen in Figure 2-b for deposits obtained from 4 M KOH at 10 mA cm^{-2}. Overgrown boulders of Zn are seen for deposits obtained from 6 M KOH at 10 mA cm^{-2} as well as those from 9 M KOH at 5 mA cm^{-2} shown in Figure 2-d and 2-e, respectively. Tree-like dendritic growth is observed for Zn deposits obtained form 9 M KOH at 10 mA cm^{-2}.

The morphology of an electrodeposited metal is greatly influenced by the deposition overpotential and, thus, current density. The magnitude of overpotential determines the free energy for nucleation. The rate of nucleation is an exponential function of the critical nucleation energy or deposition overpotential according to (11, 12):

$$\frac{dN_k}{dt} = k \cdot \exp(-\frac{\overline{\Delta G^*}}{RT}) = k_1 \exp(-\frac{k_2}{|\eta|})\ s^{-1}\ cm^{-2} \qquad [1]$$

where N_k is the number of nuclei in 1 cm^2, t the time, k and k_1 system constants, $\overline{\Delta G^*}$ the critical energy for formation of a two dimensional nucleus, R the universal gas constant, T the absolute temperature and η the overpotential. Greater overpotentials lead to higher nucleation rates and finer grain structure of the deposits as long as the process is charge-transfer-controlled.

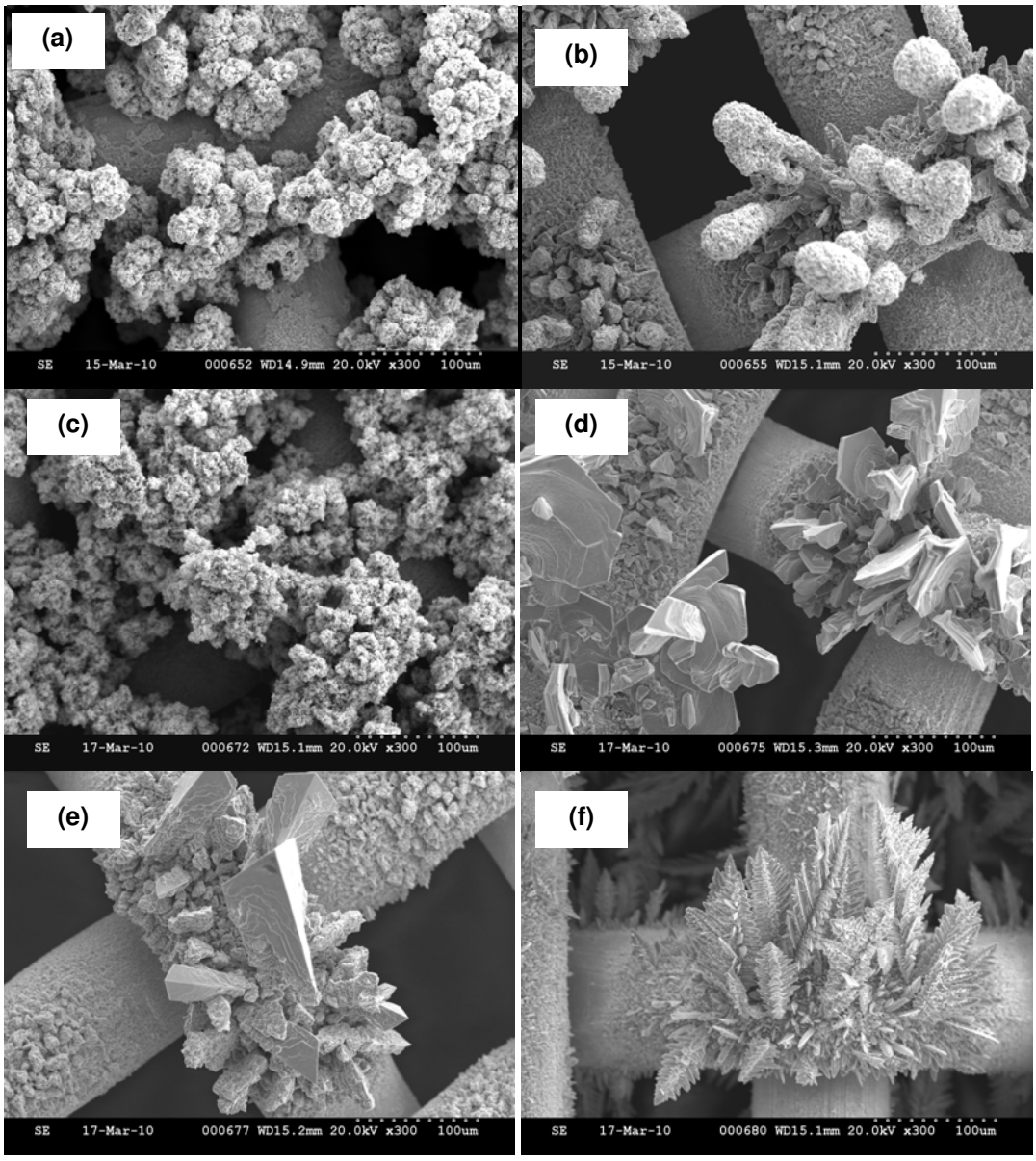

Figure 2.. Secondary electron (SE) images of Zn deposited at different conditions; (a) 4 M KOH/5 mA cm^{-2}, (b) 4 M KOH/10 mA cm^{-2}, (c) 6 M KOH/5 mA cm^{-2}, (d) 6 M KOH /10 mA cm-2, (e) 9 M KOH/5 mA cm^{-2} and (f) 9 M KOH/10 mA cm^{-2}.

The critical free energy required for one-dimensional nucleation is to a great extent less than that for two-dimensional nucleation and three-dimensional nucleation takes even more free energy to occur (11). One-dimensional point nucleation and growth of mossy deposits, consisting of convoluted filaments, may occur at low deposition overpotentials and current densities. The mossy growth which is observed in Figure 2-a and 2-d is then attributed to small deposition overpotentials (in vicinity of 25 mV in Figure 1). This type of deposit is neither adherent nor compact, and is problematic for Zn anodes.

Facet face coarse crystals, referred to as boulders, are the results of two-dimensional nucleation at moderate overpotentials (e.g., 10-100 mV depending on the system) higher than those resulting in one-dimensional nucleation (11). In the case of Zn for all KOH concentrations, in the overpotential range for two-dimensional nucleation and growth the current density would be in range that the process is either mixed-controlled or purely diffusion-controlled resulting in dendritic growth. In diffusion-controlled deposition process, the cathode diffusion layer is markedly thinner or nonexistent on the surface of asperities in comparison with valleys and recessed regions. The variation in diffusion layer thickness favors the growth of peaks where the diffusion layer is thinner or nonexistent and mass transport is not rate determining. Growth of dendrites on the convex curvatures of wires with high local current densities is a consequence of a diffusion-controlled deposition. In summary, in additive-free KOH electrolytes, deposition overpotential cannot be raised high enough to achieve a three-dimensional nucleation and compact deposits that commonly require overpotentials greater than 200 mV since the corresponding deposition current density would exceed the diffusion limiting one where the dendritic growth is certain.

Effect of duty cycle

Figure 3 shows the morphology of Zn deposits obtained at two duty cycles of 12.5% (Figure 3-a, 3-c and 3-e) and 6.25% (Figure 3-b, 3-d and 3-f) and from electrolytes containing various concentration of KOH, i.e., 4 (Figure 3-a and 3-b), 6 (Figure 3-c and 3-d) and 9 M (Figure 3-e and 3-f). The pulse frequency for all specimens was 31.25 Hz, mean current density 5 mA cm^{-2} and deposition charge 78 C. For electrolytes containing 4 and 6 M KOH (Figure 3-a to 3-d), grain refinement with reducing the duty cycle is clearly observed. However, for the Zn deposits obtained from electrolytes containing 9 M KOH, no considerable change in morphology is seen with reducing the duty cycle (figure 3-e and 3-f) and for both cases the morphology is dendritic. For deposits obtained from 4 and 6 M KOH electrolytes, facet crystals (boulders) implying two-dimensional nucleation and growth are observed for both duty cycles.

Application of pulsating current splits the cathode diffusion layer into two sub-layers, referred to as pulsating and stationary diffusion layers. The pulsating layer forms in the vicinity of cathode and the stationary layer separates the pulsating layer from the bulk electrolyte. The thickness of the pulsating diffusion layer is a function of on-time and duty cycle according to (13):

$$\delta_p = \sqrt{\frac{4}{\pi} D t_{on} (1-\theta)} \qquad [2]$$

where δ_p is the pulsating diffusion layer thickness and D is the diffusion coefficient of metallic ions in the electrolyte

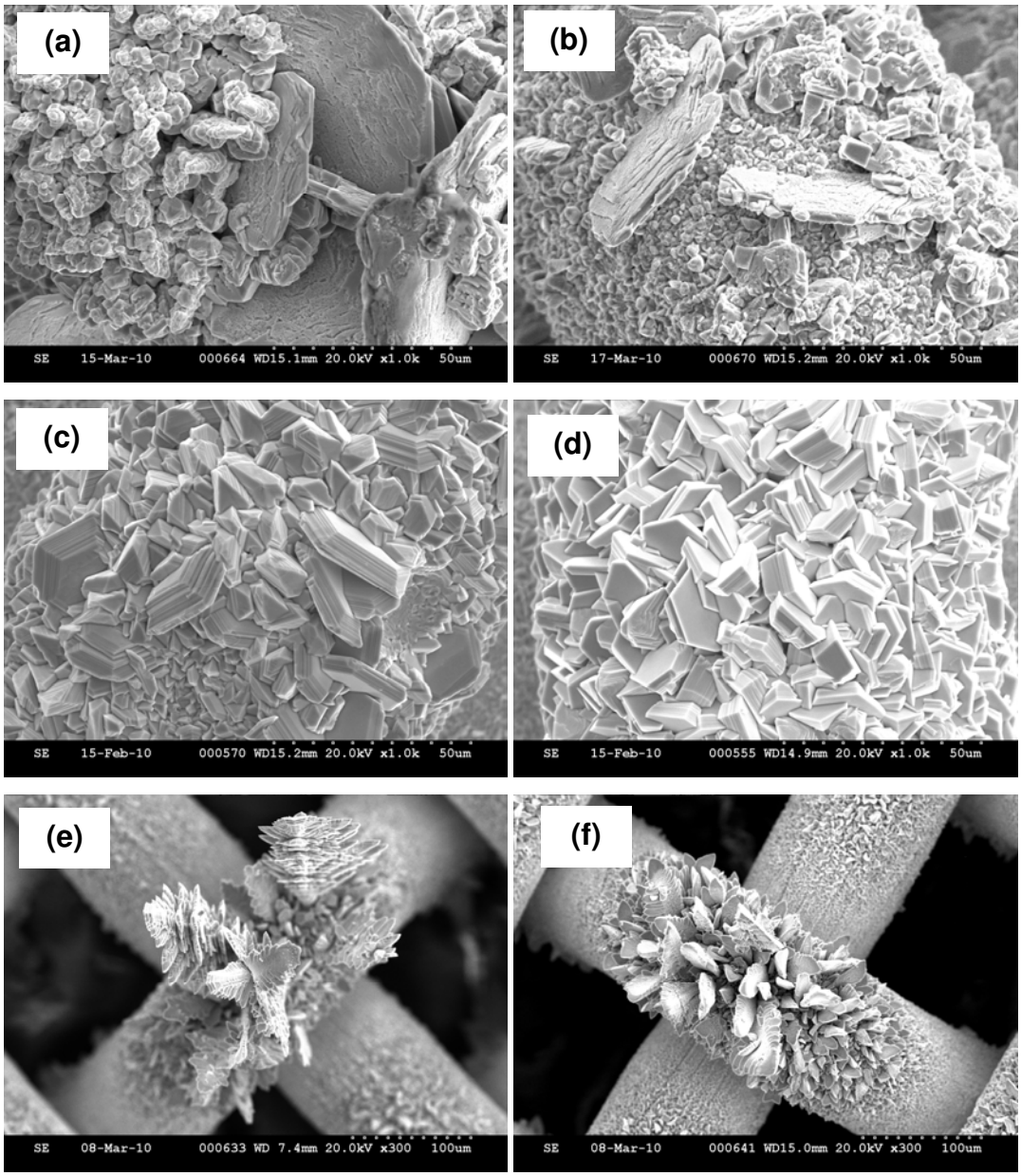

Figure 3. SE images of pulsating current deposited Zn at 31.25 Hz frequency; (a) is deposited at 12.5% duty cycle from 4 M KOH, (b) 6.25% 4 M KOH, (c) 12.5%/6 M KOH, (d) at 6.25%/6M KOH, (e) 12.5%/9 M KOH and (f) 6.25%/9 M KOH.

Smaller on-times and duty cycles give rise to a thinner pulsating diffusion layer. Formation of such a double layer reduces the limiting effect of mass transport and enables the use of high peak current densities. The ratio of the peak limiting current density to that of direct current density is again a function of on-time, diffusion layer thickness and duty cycle and can be defined as (13):

$$\frac{i_L^{PC}}{i_L^{DC}} = \left[\sqrt{\frac{4Dt_{on}}{\pi\delta^2}} (1-\theta)^{1.5} + \theta \right]^{-1} \quad [3]$$

where i_L^{PC} is the peak limiting current density in pulse deposition, i_L^{DC} the DC limiting current density and δ the diffusion layer thickness.
Smaller duty cycles enable the use of higher peak current densities and overpotentials at a given mean current density.

At all conditions, mossy growth was inhibited as high peak overpotentials changed the mode of nucleation from one-dimensional to two-dimensional. High peak current densities also result in enhanced nucleation rates and finer grains according to (1). The finer deposits obtained at 6.25% duty cycle (Figure 3-a and 3-c) as opposed to those obtained at 12.5% (Figure 3-b and 3-d) are, therefore, attributed to the higher peak current density for 6.25% duty cycle (80 mA cm^{-2}) versus 12.5 % (40 mA cm^{-2}). The absence of randomly oriented, fine crystals in all cases indicates that peak overpotentials are not yet high enough for a three-dimensional nucleation to occur, and smaller duty cycles are required to achieve that high current densities and overpotentials. The inability of the pulsating current to inhibit dendrite formation for the 9 M KOH electrolyte may be attributed to the very low limiting current density (approximately 7.5 mA cm^{-2}) and troubled ion diffusion associated with highly concentrated electrolytes.

Effect of frequency

Figure 4 shows the SEM images of Zn deposits obtained at 500 Hz frequency, 6.25% duty cycles and 5 mA cm^{-2} mean current density from electrolytes containing 4, 6 and 9 M KOH. To understand the effect of frequency, these images can be compared to those in Figure 3-b, 3-d and 3-f as the deposits were obtained at the same duty cycle (i.e., 6.25%) but higher frequency (500 Hz vs. 31.25 Hz). For 4 and 6 M KOH concentration, the effect of increasing the frequency on grain refinement is apparent. However, the Zn deposits obtained from a 9 M KOH electrolyte are dendritic.

The grain refinement observed with increasing frequency may be attributed to the effect of off-time. During the off-time, the atoms in the existing nuclei are given a time to diffuse into the larger grain. The driving force for this diffusion and disappearance of the nuclei is the lower free energy for the larger grains than that for smaller grains. The population of nuclei on the surface, therefore, decreases as the off-time increases. This may result in growth of the existing grains rather than formation of new ones. For higher frequencies, the duration of the off-time may not be long enough for diffusion and integration of the new nuclei with existing larger grains to occur. Frequency, however, cannot be increased beyond a certain point due to the effect of double layer charge and discharge periods. In case the charging time for the double layer capacitor is comparable with the on-time and the time for discharge of this layer is close to the off-time, the pulse shape changes from square to a rather sinusoidal shape. This will not allow the beneficial effects of square-wave pulses to be achieved.

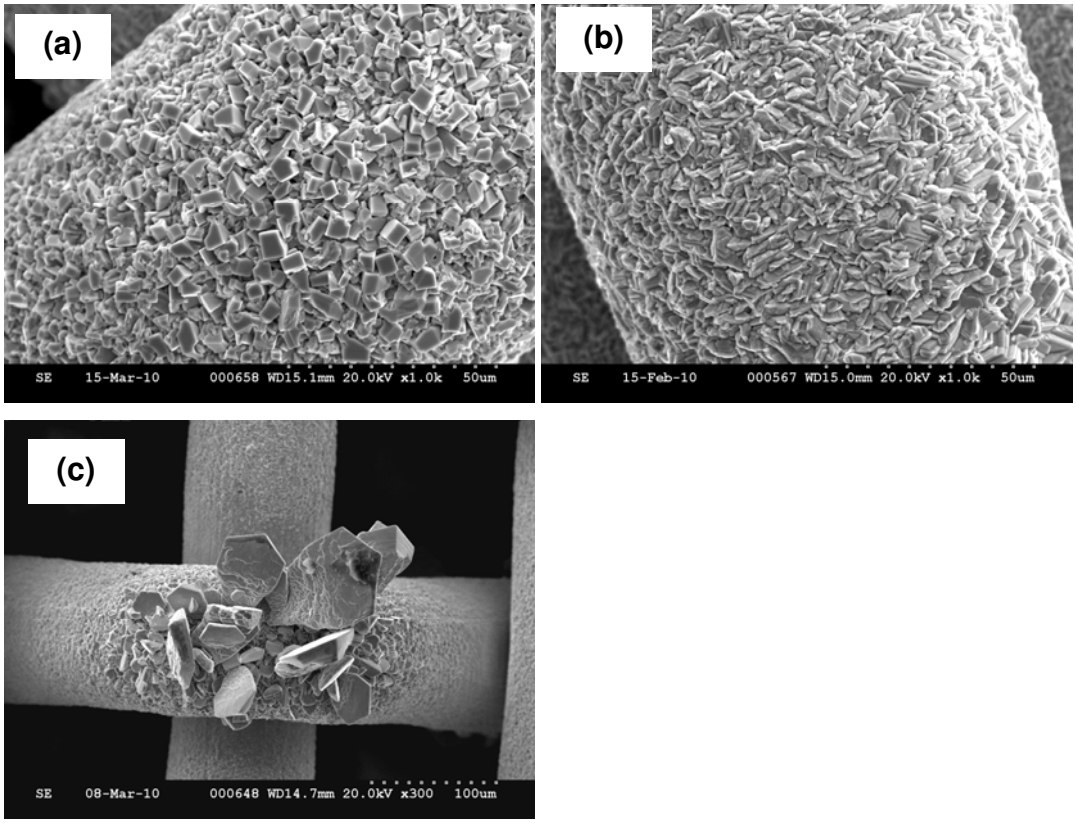

Figure 1 SE images of pulse deposited Zn at 5 mA cm^{-2} mean current density, 6.25% duty cycle and 500 Hz frequency; (a) is deposited from 4 M, (b) 6 M and (c) 9 M KOH.

Conclusions

The cathodic behavior of Zn and the effect of pulse parameters including duty cycle and frequency on morphology of the electrodeposited Zn were studied for alkaline KOH electrolytes containing zincate ions. The results showed that the Zn electrode is sharply polarized by overpotential, and activation-controlled deposition of Zn occurs at very low overpotentials (<20 mV) resulting in mossy deposits. Further increase of the overpotential results in high current densities at which the deposition is either mixed-controlled or purely diffusion-controlled and formation of dendrites is likely. In other words, three-dimensional nucleation and formation of dense deposits is unattainable for additive-free alkaline solutions using DC deposition. Mossy Zn deposits stemming from low overpotentials are inhibited by pulse deposition due to high peak current densities/overpotentials at which two-dimensional nucleation and growth occurs. Reducing the duty cycle and increasing the frequency resulted in finer grain deposits for 4 and 6 M KOH electrolytes. Virtually no improvement was observed for the 9 M electrolyte.

References

1. F. R. Mclarnon, E. J. Cairns, *J. Electrochem. Soc.*, **138**, 645 (1991).
2. XG. Zhang, *Encyclopedia of Electrochemical Power Sources,* J. Juergen, C. Dyer, P. Moseley, Z. Ogumi, D. Rand and B. Scrosati, Editors, p. 454, Elsevier, Amsterdam, (2009).
3. M. Eisenberg (Electrochimica Corporation), US Patent 4,224,391 (1980).
4. M. Eisenberg (Electrochimica Corporation), US Patent 5,215,836 (1993).
5. J. Phillips and S. Mohanta (PowerGenix Systems Inc.), US Patent 7,550,230 (2009).
6. C. Cachet, B. Saidani, R. Wiart, *J. Electrochem. Soc.*, **138**, 678 (1991).
7. C. Cachet, B. Saidani, R. Wiart, *J. Electrochem. Soc.*, **139**, 644 (1992).
8. T. P. Dirkse, N. A. Hampson, *Electrochim. Acta*, **17**, 1113 (1972).
9. T. P. Dirkse, N. A. Hampson, *Electrochim. Acta,* **17**, 383 (1972).
10. T. P. Dirkse, N. A. Hampson, *Electrochim. Acta*, **17**, 135 (1972).
11. N. Kanani, *Electroplating Basic Principles, Processes and Practice*, p. 141, Elsevier, Amsterdam, (2004).
12. J.C. Puippe, in *Theory and Practice of Pulse Plating*, J.C. Puippe and F. Leaman, Editors, p. 17, American Electroplaters and Surface Finishers Society, Orlando, (1986).
13. D. Landolt, in *Theory and Practice of Pulse Plating*, J.C. Puippe and F .Leaman, Editors, p. 55, American Electroplaters and Surface Finishers Society, Orlando, (1986).